Ultrasound in Med. & Biol., Vol. 28, Nos. 11/12, pp. 1509–1520, 2002

0301-5629/02/$–see front matter

PII: S0301-5629(02)00610-5

● *Original Contribution*

EXPERIMENTAL EVALUATION OF INDICATORS OF NONLINEARITY FOR USE IN ULTRASOUND TRANSDUCER CHARACTERIZATIONS

TIMOTHY A. BIGELOW and WILLIAM D. O'BRIEN, JR.*
Bioacoustics Research Laboratory, Department of Electrical and Computer Engineering, University of Illinois, Urbana IL, USA

(*Received* 1 *March* 2002; *in final form* 26 *July* 2002)

Abstract—Because the number of applications for medical ultrasonic devices continue to increase and, hence, the number of diagnostic ultrasound (US) systems increase, there is a need to reliably characterize the sources in terms of their output pressures. Currently, the transducers are characterized by making pressure measurements in water for every voltage range applied to the source and, then, linearly derate the measured pressure values to estimate the derated acoustic pressure levels. The process is time-consuming and inaccuracies are introduced in the derating process due to nonlinear effects. Therefore, there is a need to find an indicator of nonlinearity that could classify the measured pressure waveform as either linear, where the derating procedure would yield an accurate derated acoustic pressure estimate, or nonlinear, where the derating process would fail. Eight different indicators of nonlinearity were evaluated experimentally using spherically focused US transducers. The transducers were selected to test the indicator sensitivity to frequency (3 to 8 MHz), f-number (1 and 2), and transducer diameter (1.905 and 5.08 cm). Sensitivity to drive voltage conditions was also tested by exciting one of the transducers with pulses of different duration and phase. None of the eight nonlinearity indicators yielded consistent results. The lack of consistency resulted from the competing effects of nonlinear absorption and asymmetrical distortion, which have yet to be combined into a unified theory. (E-mail: wdo@uiuc.edu)

Key Words: **Acoustic nonlinearity, Transducer characterization, Transducer calibration.**

LIST OF SYMBOLS

α = half-angle of the transducer aperture (*i.e.*, $\sin(\alpha) = \frac{1}{2 \cdot f\#}$)

β = coefficient of nonlinearity for the medium (*i.e.*, $1 + \frac{B}{2A}$)

λ = wavelength (corresponds to ω_1)

ρ = ambient density of medium

σ = traditional nonlinear indicator for plane waves

σ_m = Bacon's nonlinear propagation parameter (absolute nonlinear indicator)

σ_s = Ostrovskii/Sutin's nonlinear propagation parameter (absolute nonlinear indicator)

σ_z = field sigma (absolute nonlinear indicator)

ω = radian frequency

ω_a = high pass cut-off frequency for absolute spectral index

ω_o = measured circuit resonance frequency for the transducer

ω_1 = frequency corresponding of maximum value of $P(\omega)$

ω_2 = frequency corresponding to the peak in the spectrum at approximately $2\omega_1$

c = small-signal sound speed of medium

dc = error introduced by circuit nonlinearities when extrapolating for p_c

dr = error introduced by circuit nonlinearities when extrapolating for p_r

da = error introduced by circuit nonlinearities when extrapolating for p_{avg}

F = focal length of spherically focused source

$f\#$ = f-number for the transducer

G = transducer gain factor resulting from focusing

G_{v_rel} = voltage gain between the current applied voltage and the low voltage reference

Address correspondence to: William D. O'Brien, Jr., Bioacoustics Research Laboratory, Department of Electrical and Computer Engineering, University of Illinois, 405 North Mathews, Urbana IL 61801. E-mail: wdo@uiuc.edu

H_{II} = second harmonic ratio (absolute nonlinear indicator)

k = wave number

P_{ae} = relative focal pressure corresponding to p_{avg} (relative nonlinear indicator)

P_{asym} = asymmetrical ratio (absolute nonlinear indicator)

p_{avg} = peak "average" pressure in pressure waveform at focus (*i.e.*, $p_{avg} = (p_c + p_r)/2$)

$p_{avg_{current}} = p_{avg}$ value for the current focal pressure waveform

$p_{avg_{low}} = p_{avg}$ value for the low voltage reference focal pressure waveform

p_c = peak compressional pressure in pressure waveform at focus

$p_{c_{current}} = p_c$ value for the current focal pressure waveform

P_{ce} = relative focal pressure corresponding to p_c (relative nonlinear indicator)

$P_{c_{low}} = p_c$ value for the low voltage reference focal pressure waveform

$P_{current}(\omega)$ = spectrum for the current focal pressure waveform

$P_{low}(\omega)$ = spectrum for the low voltage reference focal pressure waveform

p_o = pressure amplitude assumed constant across the surface of the source

p_r = peak rarefactional pressure in pressure waveform at focus

$P_{r_{current}} = p_r$ value for the current focal pressure waveform

P_{re} = relative focal pressure corresponding to p_r (relative nonlinear indicator)

$P_{r_{low}} = p_r$ value for the low voltage reference focal pressure waveform

$p(t)$ = time domain pressure waveform at the focus

$P(\omega)$ = frequency domain description of pressure waveform at focus [*i.e.*, $P(\omega) = FFT(p(t))$]

R_1, L_1, C_1, C_o = equivalent circuit parameters for a piezoelectric crystal

R_o = distance defined by Ostrovskii/Sutin that splits medium into linear and nonlinear regions of propagation

rsi = relative spectral index (relative nonlinear indicator)

si = absolute spectral index (absolute nonlinear indicator)

v_{op} = maximum amplitude voltage of the transducer drive pulse

v_{pp} = maximum peak-peak voltage of the transducer drive pulse

v_{2op} = simulated maximum amplitude voltage across R_1 of the transducer drive pulse

v_{2pp} = simulated maximum peak-peak voltage across R_1 of the transducer drive pulse

V_{sn} = magnitude of transducer drive pulse at the measured circuit resonance frequency for the transducer

V_{2sn} = magnitude of the maximum frequency component across the simulated resistor R_1

$v(t)$ = voltage pulse applied to transducer

$v_2(t)$ = simulated voltage pulse across R_1

$V(\omega)$ = Fourier transform of the voltage pulse applied to the transducer

$V_2(\omega)$ = Fourier transform of the voltage pulse across the simulated resistor R_1

x = propagation distance from plane wave source

INTRODUCTION

Over the past few decades, the propagation of acoustic signals through the human body has found application in medical imaging, as well as the treatment of various ailments. Also, many new applications are being continually developed. As the demand for medical ultrasonic devices increases, so does the demand for reliable and efficient methods of characterizing the pressure output of the ultrasound (US) transducers. Currently, for diagnostic US systems (FDA 1997), US sources are characterized by measuring the acoustic pressure in water for every voltage range applied to the source and, then, linearly derate the measured pressure values to estimate the derated acoustic pressure levels. As a result, the characterization process is time-consuming, increasing the cost and development time for each transducer. Furthermore, the derating process underestimates the true derated pressures after the heightened effects of nonlinear propagation in water have sufficiently distorted the measured pressure waveform (Christopher and Carstensen 1996; Szabo et al. 1999; Duck 1999). If the measured waveform has not been significantly corrupted by nonlinear propagation, then the traditional linear derating factor of 0.3 dB/(cm MHz) should yield a sufficiently accurate estimate of the derated acoustic pressure values. The challenge, then, is to determine if a procedure or quantity can estimate when the measured pressure waveform has not been significantly corrupted by nonlinear propagation. If such a procedure or quantity were determined, then the manufacturer could use the measured pressure for that transducer voltage setting to linearly extrapolate and derate to find the *in situ* pressure for all smaller applied voltages, reducing the overall characterization time.

Therefore, there is a need to assess the degree of nonlinearity in a measured pressure waveform during the transducer characterization process (Szabo 1999; Duck 1999). Because the goal is binary classification of the

received signal as either being linear or nonlinear, one possible approach is to find a nonlinear indicator with a consistent threshold between linear and nonlinear regions of propagation. For plane waves, the degree of nonlinearity in a waveform has been well quantified by the nonlinear indicator, σ, given by (Hamilton and Blackstock 1998):

$$\sigma = \frac{xk\beta p_o}{\rho c^2}. \tag{1}$$

If σ is less than one, the wave amplitude is consistent with that expected from linear acoustics, and nonlinear propagation can be "neglected." For higher values of σ, the waveform has been distorted beyond the point where linear acoustics could yield an adequate description. Hence, a σ value of one acts as the nonlinear indicator threshold value for the case of plane wave propagation.

For the focused fields encountered in medical US applications, the degree of nonlinear distortion is much more difficult to quantify. In general, there are two different nonlinear effects that can alter the amplitude of the pressure wave at the focus, namely, asymmetrical distortion and nonlinear absorption. Asymmetrical distortion results when diffraction and nonlinearity both act on an acoustic wave, resulting in the peak compressional pressure being larger than the peak rarefractional pressure. Although commonly observed experimentally, the only theoretical analysis of this effect in the literature was performed by Ostrovskii and Sutin (1975) and Sutin (1978). Since then, several researchers have questioned the quantitative results of their work (Lucas and Muir 1983; Bacon 1984), but no one has proposed a more complete or alternative analysis.

Nonlinear absorption is the process by which the amplitude of a propagating acoustic wave becomes independent of its source amplitude due to the nonlinear generation and subsequent absorption of harmonics (Hamilton and Blackstock 1998). Nonlinear absorption lowers both the peak compressional and the peak rarefactional pressures. Nonlinear absorption and asymmetrical pulse distortion are competing effects, with relative influences that can currently only be assessed experimentally or by the use of complicated computer models that solve the complete nonlinear acoustic equation.

To quantify the effect of these acoustic nonlinearities on the pressure waveform in water, eight different indicators of nonlinearity have been evaluated. The goal of this work was to assess these indices to determine if one of them could consistently differentiate between the linear and nonlinearly corrupted pressure waveforms. To this end, each of the indices was evaluated experimentally for a series of spherically focused transducers under different drive-voltage conditions. Spherical transducers were selected as opposed to the arrays commonly encountered in medical US due to their simpler theoretical analysis. Also, if the performance of the indicators were not adequate for the fields produced by spherical transducers, then they would also fail for the more complicated fields produced by array transducers. Some of the indicators evaluated herein were specifically derived for the spherically focused sources; however, equivalent indicators for arrays could be found by an appropriate theoretical analysis if desired.

The first step in assessing any type of nonlinear indicator is to determine how the value of the indicator is to be compared to the amount of distortion in the pressure pulse. The distortion of the pulse was quantified by back-extrapolating the pressure values, p_c, p_r, and p_{avg}, from the current drive voltage applied across the transducer to all lower applied voltages. The maximum error between the extrapolated pressures and the actual measured pressures at the lower voltages was then used to quantify the amount of distortion in the pressure pulse, the same type of distortion that would also corrupt the linearly derated pressure amplitudes. The break (binary classifier) between linear and nonlinear propagation was defined to correspond to an extrapolation error of 10%. Hence, nonlinear indicator values corresponding to the 10% level of distortion were identified as the threshold nonlinear indicator value for a particular transducer and drive-voltage condition. The ideal nonlinear indicator would yield the same threshold value regardless of the frequency, focal length, f-number or type of voltage excitation. Also, the indicator would achieve this threshold value at only one excitation condition (*i.e.*, the indicator should be monotonic). Hence, in our experiment, threshold values for each of the proposed indicators were evaluated based on these ideal criteria.

In this paper, each of the indicators will be defined. Then, the experimental procedure followed to obtain the threshold values of the nonlinear indicators will be discussed, and the experimental results will be presented. Last, some conclusions will be drawn based on the results. More details on the specifics of this investigation can be found in Bigelow (2001).

BACKGROUND OF EVALUATED INDICES

The indices evaluated herein can be grouped into two categories, absolute indicators of nonlinearity and relative indicators of nonlinearity. The relative indicators incorporate into the analysis information from the pressure waveform at an arbitrary low-voltage measurement of the same transducer, whereas the absolute indicators only require information from the present drive-voltage

setting. The low-voltage measurement for the relative indicators was not used for any type of extrapolation during the assessment of the nonlinear indicators. It merely served as a reference so that changes in the waveform would be easier to quantify. The low-voltage measurement was always taken to be the pressure waveform from the lowest drive-voltage applied to the transducer. The absolute indicators of nonlinearity are the asymmetrical ratio, Ostrovskii/Sutin's propagation parameter σ_s, Bacon's acoustic propagation parameter σ_m, the field sigma σ_z, the second harmonic ratio, and the absolute spectral index. The relative indicators of nonlinearity are the relative spectral index and the relative focal pressure.

Asymmetrical ratio

Because asymmetrical distortion is an effect induced by nonlinear propagation, it would seem that a logical choice for an indicator should reflect the amount of asymmetry in the waveform. One quantity that does this is the asymmetrical ratio given by:

$$P_{asym} = \frac{P_c}{P_r}. \tag{2}$$

The asymmetrical ratio was first proposed for use as a nonlinear indicator by Szabo et al. (1999).

Ostrovskii/Sutin's propagation parameter σ_s

The amount of asymmetrical distortion in a waveform can also be described by Ostrovskii/Sutin's propagation parameter σ_s (Ostrovkii and Sutin 1975). The larger the value of σ_s, the more nonlinear the waveform. σ_s is defined as:

$$\sigma_s = \frac{p_o \omega_1 F \beta}{\rho c^3} \ln\left(\frac{F}{R_o}\right). \tag{3}$$

The distance R_o is an arbitrary distance defined by Ostrovskii/Sutin that splits the medium into two regions of propagation. These regions are the nonlinear region away from the focus where diffraction effects are ignored (i.e., distance from focus $> R_o$) and the focal region where diffraction effects are included, but nonlinear propagation is neglected (*i.e.*, distance from focus $< R_o$). The value of R_o is difficult to define quantitatively. For this work, the value selected was (Ostrovskii and Sutin 1975):

$$R_o = \frac{\lambda}{1 - \cos(\alpha)}. \tag{4}$$

The Ostrovskii/Sutin method assumes small nonlinearities and does not take into account nonlinear absorption.

Although defined by eqn (3), σ_s cannot be found in this manner because the initial source pressure, p_o, is not known from a measurement made at the focus. One method for removing the dependence on p_o is to use Ostrovskii/Sutin's theory to express p_o as a function of the expected rarefactional pressure at the focus. A simple substitution then yields:

$$\sigma_s = \frac{p_r \beta \ln\left(\frac{F}{R_o}\right)}{2\rho c^2 \left(\frac{\alpha \cdot \sin(\alpha)}{\pi}\right) - \left(p_r \beta \ln\left(\frac{F}{R_o}\right)\right)}. \tag{5}$$

Another method for determining σ_s that is independent of p_o that also avoids the uncertainty in R_o is based on the asymmetrical ratio. Assuming the values for p_c and p_r predicted by Ostrovskii/Sutin's theory are valid, then substitution also yields a σ_s, given by:

$$\sigma_s = \frac{P_{asym} - 1}{P_{asym} + 1}. \tag{6}$$

In our investigation, σ_s was calculated and evaluated as a nonlinear indicator using both eqns (5) and (6).

Bacon's propagation parameter σ_m

A nonlinear indicator that is also currently considered a standard measure of nonlinearity is Bacon's acoustic propagation parameter σ_m (Szabo et al. 1999; Duck 1999). The goal of Bacon's analysis was very similar to our present analysis, in that he wanted to determine the amount of nonlinearity in a converging sound wave based on a pressure measurement at the focus. Bacon's σ_m is given by (Bacon 1984):

$$\sigma_m = \frac{\beta \omega_1 p_{avg} F}{\rho c^3} \frac{\ln(G + \sqrt{G^2 - 1})}{\sqrt{G^2 - 1}}, \tag{7}$$

where G was the ratio of the amplitude at the focus to the amplitude of the intersection of the beam axis with the transducer surface. Unfortunately, this value cannot be measured explicitly. Bacon attempts to provide a method for determining G by stating that the ratio of the aperture area of the transducer to the area of the beam at the focus should be G. However, these areas cannot be consistently defined. If one uses the -6-dB focal area as proposed by Bacon, then, to be consistent with Bacon's theory, the -6-dB locus should also be used in the aperture plane of the transducer. Therefore, in our analysis, G was simply calculated by assuming an ideal spherically focused source yielding:

$$G = \sqrt{\left(\frac{F}{\pi \lambda (0.8224 \cdot (f\#))^2}\right)^2 + 1}. \tag{8}$$

Field sigma σ_z

Another nonlinear indicator that neglects the dependence on transducer gain that was originally proposed by Szabo et al. (1999) is the field sigma, σ_z, given by:

$$\sigma_z = \frac{\beta \omega_1 p_{avg} F}{\rho c^3}. \tag{9}$$

Notice that eqn (9) is the same as eqn (7) for σ_m with the G terms removed. This oversimplification of σ_m places the entire basis for σ_z in a rather precarious position. It would seem highly unlikely for σ_z to properly reflect the amount of nonlinear distortion in a waveform for all possible transducer gains.

Second harmonic ratio

For the previously proposed indices, the amount of nonlinearity in the waveform at the focus was determined based on pressure measurements made in the time domain. However, nonlinear propagation also transfers energy out of the fundamental frequency and into the higher harmonics (Hamilton and Blackstock 1998; Naugolnykh and Ostrovsky 1998; Pierce 1991). Therefore, another nonlinear indicator also proposed by Szabo et al. (1999) is the second harmonic ratio given by

$$H_{II} = \frac{|P(\omega_2)|}{|P(\omega_1)|}, \tag{10}$$

where ω_1 is the principle frequency of the sound pulse, and ω_2 corresponds to the peak in the spectrum at approximately $2\omega_1$ as illustrated by Fig. 1. Notice that, in these plots, ω_2 is not exactly $2\omega_1$. This can be attributed to higher attenuation at the higher frequencies (Pierce 1991).

Absolute spectral index

Another possible nonlinear indicator that would reflect the generation of harmonics by nonlinear propagation is the absolute spectral index. The absolute spectral index was originally proposed by Duck (1999), and is defined as:

$$si = \frac{\int_{\omega_a}^{\infty} |P(\omega)| d\omega}{\int_{0}^{\infty} |P(\omega)| d\omega}. \tag{11}$$

The frequency ω_a is an arbitrary frequency that is selected with the intent of including in the numerator integral only the frequencies generated by nonlinear propagation. Ideally, the *si* would be zero in the absence of nonlinear effects, and then grow as higher harmonics were generated by nonlinear propagation. For our analysis, we considered two possible choices for ω_a: $2\omega_1$ and $1.5\omega_1$. Duck (1999) suggested using an ω_a corresponding to the upper frequency of the −6-dB bandwidth. However, our preliminary results indicated that the performance of the *si* did not vary significantly for these different choices of ω_a, so only $2\omega_1$ and $1.5\omega_1$ were included in the rigorous analysis.

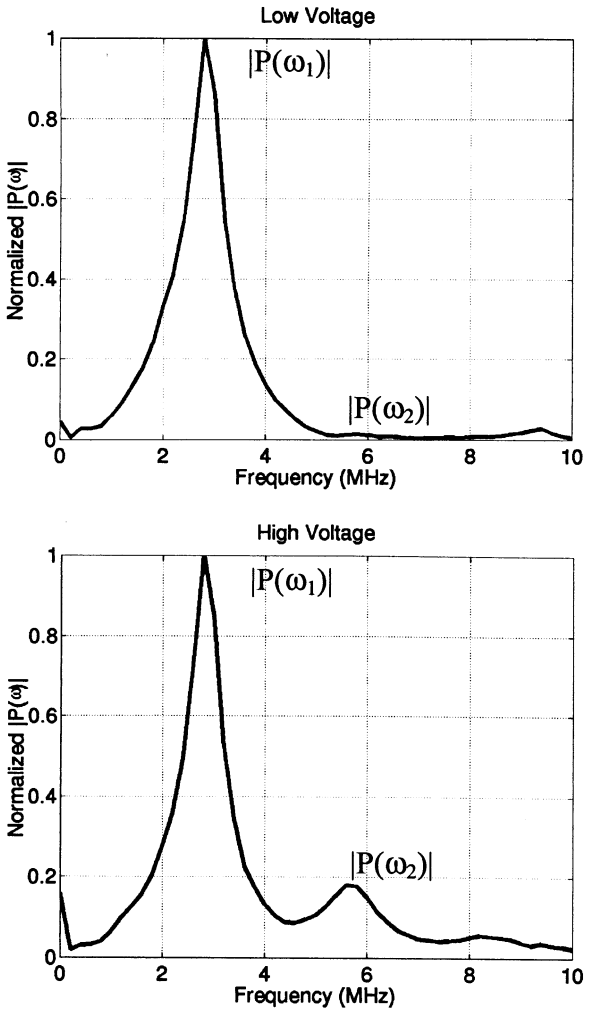

Fig. 1. Typical frequency spectrum at the focus of a spherically focused transducer under two different drive conditions.

Relative spectral index

The previous six nonlinear indicators were absolute indicators of nonlinearity; however, a relative indicator may be able to better quantify the pulse distortion intro-

duced by nonlinear propagation. The relative spectral index is a relative indicator that monitors all changes in the amplitude spectrum of the acoustical signal. The relative spectral index is given by:

$$rsi = \frac{\int_0^{\infty} (|P_{\text{current}}(\omega)| - G_{v\_\text{rel}}|P_{\text{low}}(\omega)|)^2 d\omega}{\int_0^{\infty} |P_{\text{current}}(\omega)|^2 d\omega}. \quad (12)$$

Unlike the second harmonic ratio, H_{II}, and the absolute spectral index, *si*, which focus on the generation of higher harmonics, the relative spectral index has the luxury of capturing all changes in the spectrum including the generation of subharmonics (Hamilton and Blackstock 1998) and nonlinear absorption.

Relative focal pressure

The relative focal pressure captures the effects of nonlinear distortion by comparing the pressure amplitudes of the current measured waveform to the reference waveform in the time domain. Because the pressure amplitude of the pulse can be characterized by three different quantities, p_c, p_r, and p_{avg}, three different values for the relative focal pressure are defined:

$$P_{\text{ce}} = 100 \cdot \left| \frac{p_{\text{c}_{\text{current}}} - G_{v\_\text{rel}} p_{\text{c}_{\text{low}}}}{p_{\text{c}_{\text{current}}}} \right| \quad (13)$$

$$P_{\text{re}} = 100 \cdot \left| \frac{p_{\text{r}_{\text{current}}} - G_{v\_\text{rel}} p_{\text{r}_{\text{low}}}}{p_{\text{r}_{\text{current}}}} \right| \quad (14)$$

$$P_{\text{ae}} = 100 \cdot \left| \frac{p_{\text{avg}_{\text{current}}} - G_{v\_\text{rel}} p_{\text{avg}_{\text{low}}}}{p_{\text{avg}_{\text{current}}}} \right| \quad (15)$$

EXPERIMENTAL PROCEDURE

The excitation system formed the backbone of the measurement system (Fig. 2). It generated the high-magnitude drive-voltage pulse that would be transmitted by the spherically focused US transducer (Matec/Valpey Fisher Instruments, Inc., Hopkinton, MA) as an acoustic wave. The pulse-generating system consisted of a computer-controlled high-power pulsed source (RAM5000, Ritec, Inc., Warwick, RI). The controllable parameters were the phase of the pulse, the center frequency of the pulse, the number of cycles in the pulse and the amplitude. The phase of the pulse refers to the phase of the sinusoid output by the pulse generator. Hence, a phase of 0^{o} would generate a pulse that started at 0 V and then

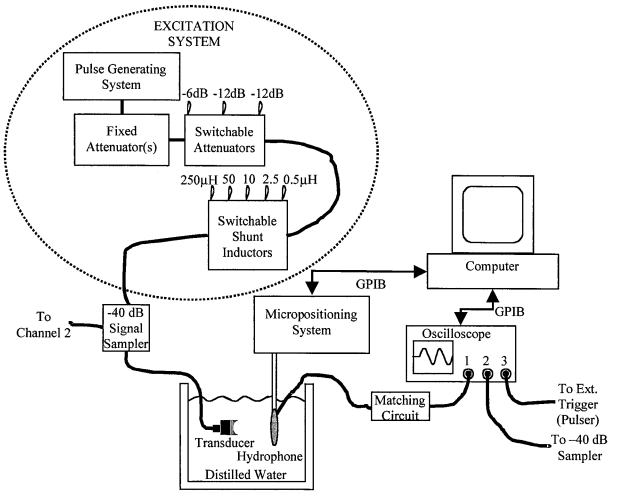

Fig. 2. Diagram of experimental setup.

increased (*i.e.*, "positive going"), whereas a phase of 180^{o} would generate a pulse that started at 0 V and then decreased (*i.e.*, "negative going"). The pulse amplitude was set by selecting a RAM5000 amplitude level in the range from 1 to 100 that the system translated into a voltage. The relationship between the selected amplitude level and the resulting drive-voltage was roughly linear.

The control parameters of center frequency and number of cycles refer to the selected primary frequency of the pulse and the selected number of complete cycles in the drive-voltage pulse. The RAM5000 pulse generator was designed so that the cycles would all be of equal amplitude, emulating a sinusoid at the pulse frequency windowed by a rectangular window. However, the RAM5000 was designed to drive a 50-Ω load. Therefore, when the pulse generator was connected to the reactive load of the transducer, the performance of the generator was degraded. Specifically, the number of cycles, frequency content and linearity between different amplitude pulses were severely affected. As a result, attenuators and inductors were included in the signal path to improve the performance of the source, but the properties of the transmitted waveform were still not a perfect reproduction of the values selected by the computer. However, in this paper, "drive condition" still refers to the number of cycles, frequency and phase set by the computer for a particular transducer.

After it was generated, the acoustic pulse would then travel through the highly degassed water (~ 20°C) to the calibrated PVDF membrane hydrophone (Marconi, Ltd., Essex, UK), which would translate it back into a voltage signal to be read by channel one on the digital oscilloscope (LeCroy Model 9354TM, Chestnut Ridge, NY). Channel 2 of the oscilloscope was used to monitor the drive-voltage pulse applied to the transducer *via* a

−40-dB signal sampler (SS-40, Ritec, Inc.). The oscilloscope would then digitize the waveforms at a sampling rate of 500 MHz and perform the average over 100 pulses before sending the results to the computer (Dell Pentium-II). The computer saved the temporal waveforms for off-line analysis and controlled the precision positioning system (Daedal Inc., Harrison City, PA) that was used to maneuver the hydrophone.

The experiment was comprised of a series of data sets designed to test the performance of each of the nonlinear indicators. Because the goal was to find an indicator that would be applicable to any focused source under any drive condition, many different types of transducers and excitations were evaluated. To test insensitivity to frequency, transducers were selected with circuit resonant frequencies of approximately 3 MHz, 5.5 MHz and 8 MHz. Also, to confirm insensitivity to *f*#, transducers with *f*#'s of 1 and 2 were evaluated. Aperture size was also tested by selecting transducers with approximately the same frequency and *f*#, but having different diameters. Furthermore, insensitivity to drive conditions was tested by driving one of the transducers with a positive-going three-cycle pulse, a negative-going three-cycle pulse, and a positive-going one-cycle pulse. For each transducer, the principal output frequency selected with the computer corresponded to the circuit resonant frequency of the transducer. The circuit resonant frequencies were measured by an HP Network Analyzer before the acoustic measurement.

Each data set consisted of a series of measurements that recorded the pressure waveform "close" to the transducer, the pressure waveform at the focus of the transducer, and the drive-voltage pulse waveform applied across the transducer for a series of amplitude settings. The waveform from the "close" location was obtained by moving the hydrophone as close as possible to the aperture of the transducer ($\sim$ 1 mm of separation) approximately along the beam axis. The close waveform was principally used to select the best drive-voltage–based extrapolation factor for the measurements. The same analysis also quantified the linearity of the excitation system and, hence, was used to set confidence measures for the threshold values of the nonlinear indicators.

The focal pressure waveform was used to determine and assess the performance of the different nonlinear indicators. Traditionally, the focus of diagnostic US systems has been defined as the location of the derated maximum pulse intensity integral (PII) (FDA 1997; AUIM/NEMA 1998; Sempsrott and O'Brien 1999; Sempsrott 2000). However, this quantity cannot generally be directly observed on an oscilloscope. Therefore, for this investigation, the focus for each of the transducers was taken to be the location where the peak-peak voltage, as reported by the hydrophone while exciting the transducer with a low drive-voltage pulse, was maximum. Because the shift of the focus due to nonlinear propagation is a relatively minor effect, the focal location was assumed to be a constant independent of drive-voltage for each of the transducers.

Within each data set, the drive-voltage applied to the transducer (*i.e.,* the amplitude setting) was varied by changing the amplitude of the pulse selected by the computer in the pulse generator and by changing the variable attenuator settings. All the measurements for a given transducer and drive condition were obtained before any changes were made in either the transducer or the drive conditions.

EXPERIMENTAL RESULTS

Extrapolation factor analysis

Recall that the principle goal of this investigation was to evaluate the ability of the different nonlinear indicators to distinguish between linear and nonlinear-corrupted focal pressure waveforms. Also, the amount of nonlinear distortion in a focal waveform was quantified by the error between the true focal pressures and the pressures predicted by back-extrapolating from the current focal waveform for all smaller applied voltages. However, for the back-extrapolation to be valid, the spectrum of the drive-voltage pulse must also vary linearly as the drive amplitude is increased. Furthermore, the amplitude of the drive-voltage pulse can be assessed by a variety of measures. In the ideal case, all of the measures would yield the same degree of linearity. However, this is not the case, and some of the measures will minimize the effect of the circuit nonlinearities. Therefore, the first step in analyzing our results was to find the best possible candidate for the extrapolation factor.

Six measures of the drive-voltage pulse were introduced as possible candidates for the extrapolation factor. The different measures could be grouped into three distinct categories, with each category contributing two possible extrapolation factors. The first category consisted of direct voltage measurements of the drive-voltage pulse. In this category, the two extrapolation factors were the maximum amplitude voltage of the drive pulse, v_{op}, and the maximum peak-peak voltage of the drive pulse, v_{pp}, each of which was determined by:

$$v_{\mathrm{op}} = \max_{t \epsilon \mathrm{pulse}}(|v(t)|) \tag{16}$$

$$v_{\mathrm{pp}} = \max_{t \epsilon \mathrm{pulse}}(v(t)) - \min_{t \epsilon \mathrm{pulse}}(v(t)) \tag{17}$$

where the notations $\max_{t \epsilon \mathrm{pulse}}(v(t))$ and $\min_{t \epsilon \mathrm{pulse}}(v(t))$ refer to the maximum and minimum values of $v(t)$ for all t in the measured acoustic pulse, respectively.

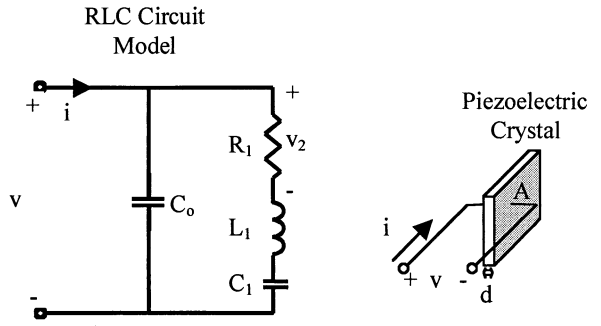

Fig. 3. Equivalent RLC circuit model for a piezoelectric transducer.

The second category of extrapolation factors consisted of circuit-based voltage measurements. The drive-voltage pulse across the transducer was filtered analytically to capture the true pressure spectrum being radiated by the transducer. In this way, the extrapolation would not be effected by nonlinearities in the drive-voltage pulse at frequencies outside of the range of interest. However, nonlinearities in frequencies radiated by the transducer would still corrupt the ability to perform linear extrapolation. The filtering approach is based on the idea that every piezoelectric transducer can be modeled as the equivalent RLC circuit (Fig. 3) when excited near its fundamental resonant frequency (Bechmann and Fair 1966).

In this circuit, the voltage v_2 across the resistor R_1 corresponds to the acoustic signal radiated by the piezoelectric crystal, as well as other losses that might be present in the crystal. The reactive elements L_1 and C_1 capture the resonant behavior of the crystal. Also, the capacitor C_o is the capacitance resulting from the fact that the transducer consists of a dielectric, the piezoelectric crystal, between two excited conducting surfaces. Each of these circuit parameters was obtained experimentally for each transducer using S_{11} reflection measurements from an HP Network Analyzer. The reflection measurements yielded the input impedance of the transducer for many different frequency values, from which the circuit parameters could then be fitted.

The two circuit-based extrapolation factors considered were the maximum amplitude voltage across R_1, v_{2op}, and the maximum peak-peak voltage across R_1, v_{2pp}, each of which was determined from:

$$v_{2_{op}} = \max_{t \epsilon \text{pulse}}(|v_2(t)|) \tag{18}$$

$$v_{2_{pp}} = \max_{t \epsilon \text{pulse}}(v_2(t)) - \min_{t \epsilon \text{pulse}}(v_2(t)) \tag{19}$$

where $v_2(t)$ is determined from:

$$v_2(t) = IFFT\left\{ V(\omega) \frac{R_1 \omega C_1}{R_1 \omega C_1 + j(\omega^2 L_1 C_1 - 1)} \right\}. \tag{20}$$

In all four of the extrapolation factors from the first two categories, the factor was based on a time-domain measure of the drive-voltage waveform. For the third category of extrapolation factors, the factor was based on a frequency-domain measure of the drive-voltage waveform. The first factor is the magnitude of the drive waveform at the measured circuit resonance frequency for the transducer, given by:

$$V_{sn} = |V(\omega_o)| \tag{21}$$

This factor would directly relate to the pulse radiated by the transducer, like the circuit-based factors discussed above; however, it would be less sensitive to errors in the values of the circuit parameters. Another possible frequency-domain extrapolation factor is the magnitude of the maximum frequency component across the simulated resistor R_1:

Table 1. Evaluation of extrapolation factors for p_c quantified in terms of the mean extrapolation error determined from the "close" pressure waveforms

Transducer *f*# (diameter)	Resonant frequency	Drive pulse	% Error w/v_{op}	% Error w/v_{pp}	% Error w/v_{2op}	% Error w/v_{2pp}	% Error w/V_{sn}	% Error w/V_{2sn}
1 (1.905 cm)	2.81 MHz	3, p	1.93	2.31	2.79	2.81	2.62	2.55
1 (5.08 cm)	3.00 MHz	3, p	1.28	1.57	1.43	1.44	1.46	1.20
1 (1.905 cm)	5.49 MHz	1, p	2.67	2.12	2.63	2.89	5.19	4.05
1 (1.905 cm)	5.49 MHz	3, p	1.92	1.96	2.05	2.07	2.07	1.87
1 (1.905 cm)	5.49 MHz	3, n	3.72	3.28	3.38	3.41	3.42	3.21
2 (1.905 cm)	5.36 MHz	3, p	3.16	3.37	2.97	3.02	3.34	2.95
1 (1.905 cm)	8.15 MHz	3, p	5.13	5.05	5.32	4.99	4.90	5.01

"Drive pulse" refers to the properties of the drive-voltage pulse selected with the computer. The number (*i.e.*, 1 or 3) refers to the selected number of cycles in the drive-voltage pulse, and the letter (*i.e.*, p or n) refers to whether the pulse was positive-going or negative-going.

Table 2. Evaluation of extrapolation factors for p_r quantified in terms of the mean extrapolation error determined from the "close" pressure waveforms

Transducer *f*# (diameter)	Resonant frequency	Drive pulse	% Error w/v_{op}	% Error w/v_{pp}	% Error w/v_{2op}	% Error w/v_{2pp}	% Error w/V_{sn}	% Error w/V_{2sn}
1 (1.905 cm)	2.81 MHz	3, p	1.14	1.59	1.84	1.86	1.66	1.58
1 (5.08 cm)	3.00 MHz	3, p	1.10	1.68	1.49	1.52	1.54	1.27
1 (1.905 cm)	5.49 MHz	1, p	2.52	1.99	1.85	1.59	3.85	2.65
1 (1.905 cm)	5.49 MHz	3, p	2.18	1.76	1.61	1.59	1.76	1.67
1 (1.905 cm)	5.49 MHz	3, n	2.41	1.85	1.53	1.48	1.72	1.52
2 (1.905 cm)	5.36 MHz	3, p	1.85	1.78	1.56	1.56	2.02	1.79
1 (1.905 cm)	8.15 MHz	3, p	1.61	1.28	1.62	1.24	1.25	1.31

"Drive pulse" refers to the properties of the drive-voltage pulse selected with the computer. The number (*i.e.*, 1 or 3) refers to the selected number of cycles in the drive-voltage pulse, and the letter (*i.e.*, p or n) refers to whether the pulse was positive-going or negative-going.

$$V_{2sn} = \max_{\forall \omega} |V_2(\omega)|. \tag{22}$$

The different candidates for the extrapolation factor were evaluated using the pressure waveforms obtained with the hydrophone "close" to the transducer, assuming that nonlinear propagation effects could be ignored at this distance. The evaluation was done by finding the mean extrapolation error on the "close" pressure waveforms using each of the possible extrapolation factors. The extrapolation was forward extrapolation, using as a reference waveform the lowest drive-voltage setting at which the quantization effects introduced by the scope were negligible. The resulting mean errors are tabulated (Tables 1, 2 and 3) for each of the extrapolation factors.

From the results presented in the Tables, all of the error values are on the order of 2% to 5%, and all are approximately the same. This means that our system is sufficiently linear so that any one of the candidates could be selected for the extrapolation voltage. Unfortunately, this also makes it somewhat difficult to select the best extrapolation factor from the six that were evaluated. To make a choice, a scoring scheme was implemented, where the minimum value of each row was worth 2 points, each second minimum 1 point, each maximum -2 points, and each second maximum -1 point. The scoring scheme emphasized the performance of each factor within the individual data sets. Based on this scoring scheme, V_{2sn}, eqn (22) had the highest score and, hence, was selected as the extrapolation factor for the rest of the analysis. Recall that V_{2sn} was the voltage at the maximum frequency component across the simulated resistor R_1. Before concluding this discussion, it is important to mention that, although V_{2sn} yielded the best performance for the excitation system, it remains to be shown if this extrapolation factor would also be the best choice for other systems.

Nonlinear indicator analysis

Now that the extrapolation factor has been defined, the processing of the data to determine the threshold values for the different indices needs to be explained. For the experiments, the threshold between linear and nonlinear waveforms was defined to occur at a back-extrapolation error of 10%. Back-extrapolation was selected over forward-extrapolation so that the measurement would not be influenced by the choice of the smallest excitation pulse applied to the transducer. Also, back-extrapolation could be performed to 0 applied voltage by fitting a polynomial to the extrapolation error data points.

Table 3. Evaluation of extrapolation factors for p_{avg} quantified in terms of the mean extrapolation error determined from the "close" pressure waveforms

Transducer *f*# (diameter)	Resonant frequency	Drive pulse	% Error w/v_{op}	% Error w/v_{pp}	% Error w/v_{2op}	% Error w/v_{2pp}	% Error w/V_{sn}	% Error w/V_{2sn}
1 (1.905 cm)	2.81 MHz	3, p	1.34	1.80	2.34	2.34	2.13	2.06
1 (5.08 cm)	3.00 MHz	3, p	1.15	1.61	1.46	1.48	1.48	1.29
1 (1.905 cm)	5.49 MHz	1, p	2.38	1.81	1.99	2.22	4.57	3.39
1 (1.905 cm)	5.49 MHz	3, p	1.59	1.33	1.22	1.22	1.35	1.22
1 (1.905 cm)	5.49 MHz	3, n	2.72	2.13	2.25	2.28	2.28	2.11
2 (1.905 cm)	5.36 MHz	3, p	2.34	2.50	2.17	2.21	2.46	2.13
1 (1.905 cm)	8.15 MHz	3, p	3.23	3.17	3.51	3.10	3.06	3.21

"Drive pulse" refers to the properties of the drive-voltage pulse selected with the computer. The number (*i.e.*, 1 or 3) refers to the selected number of cycles in the drive-voltage pulse, and the letter (*i.e.*, p or n) refers to whether the pulse was positive-going or negative-going.

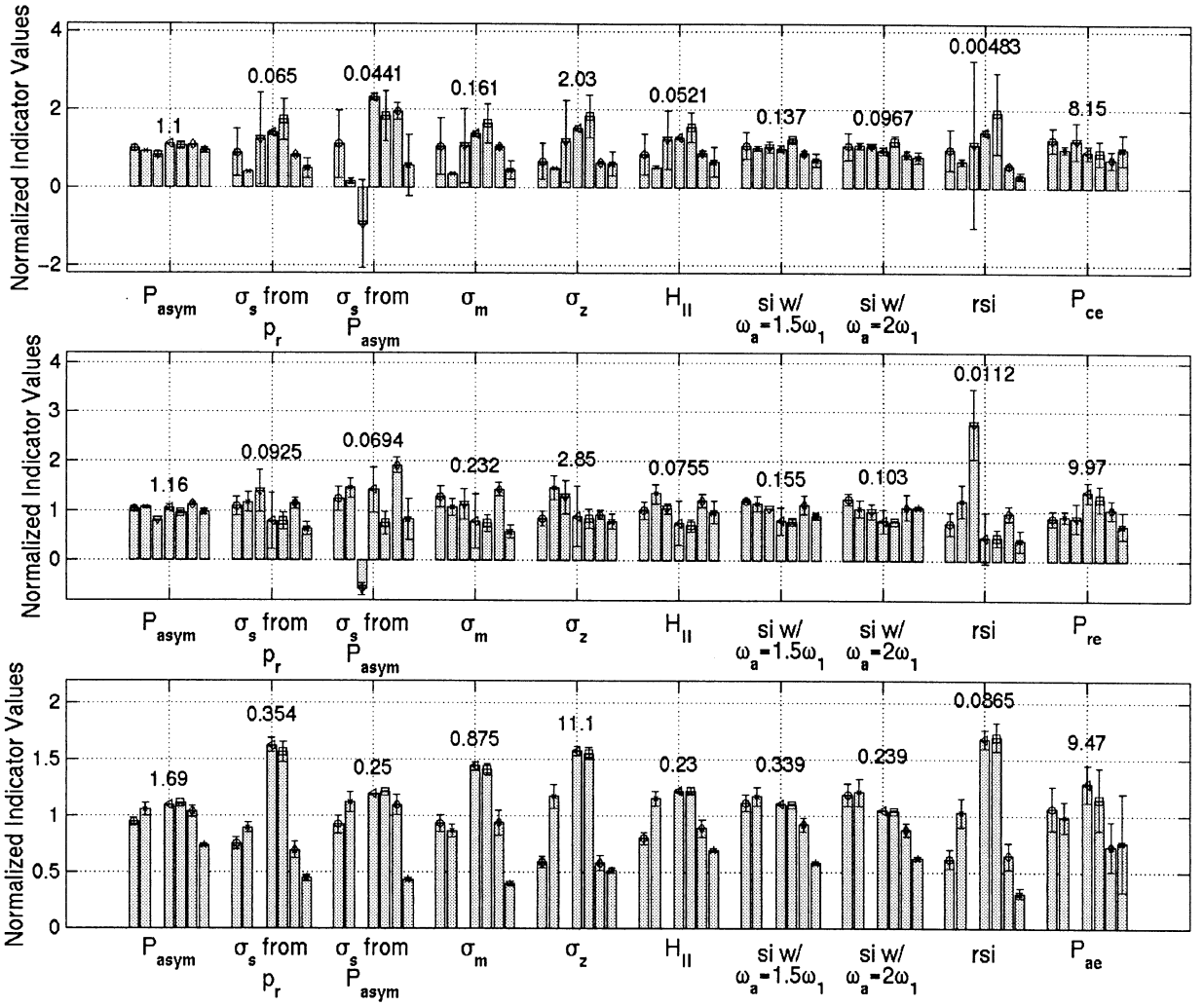

Fig. 4. Normalized threshold values for the nonlinear indicators for (top) p_c, (middle) p_r and (bottom) p_{avg}. The mean value for each indicator is provided above the corresponding bars. Within each indicator group, o corresponds to the ~ 3-MHz, *f*# of 1, 1.905-cm-diameter transducer driven with a three-cycle positive-going pulse; x corresponds to the ~ 3-MHz, *f*# of 1, 5.08-cm diameter transducer driven with a three-cycle positive-going pulse; σ corresponds to the ~ 5.5-MHz, *f*# of 1, 1.905-cm diameter transducer driven with a one-cycle positive-going pulse; ↓ corresponds to the ~ 5.5-MHz, *f*# of 1, 1.905-cm diameter transducer driven with a three-cycle positive-going pulse; ♦ corresponds to the ~ 5.5-MHz, *f*# of 1, 1.905-cm diameter transducer driven with a three-cycle negative-going pulse; ↓ corresponds to the ~ 5.5-MHz, *f*# of 2, 1.905-cm diameter transducer driven with a three-cycle positive-going pulse; and·corresponds to the ~ 8-MHz, *f*# of 1, 1.905-cm diameter transducer driven with a three-cycle positive-going pulse.

The threshold value of 10% was chosen because the error in directly measuring the pressure values was often of this same order (Sempsrott and O'Brien 1999; Sempsrott 2000).

For each data set, a 10% threshold value of the extrapolation factor, V_{2sn}, was found by determining when the back-extrapolation error first exceeded the 10% threshold error level *via* a basic root-finding technique. The back-extrapolation errors for extrapolation voltages between the experimentally applied drive-voltages was found by doing a cubic B-spline fit to the measured p_c, p_r, p_{avg} vs. V_{2sn} data points. Cubic B-spline interpolation of the threshold values of the nonlinear indices vs. V_{2sn} then yielded the threshold values of the indices at the threshold extrapolation factor.

Furthermore, because the principal source of error in the analysis would be the circuit nonlinearities that were assessed by the "close" pressure measurements, confidence measures for each of the threshold indicator values for each data set can be determined. Let *dc*, *dr*, and *da* correspond to the errors as reported in the last column of Tables 1, 2 and 3, respectively. Then, confi-

dence error bars were found by repeating the process for finding the threshold values of the nonlinear indicators with the threshold error changed from 10% to 10% $\pm$ $dc/2$, 10% $\pm$ $dr/2$ and 10% $\pm$ $da/2$ for the p_c, p_r, and p_{avg} values, respectively.

The normalized threshold values for the eight nonlinear indicators, together with the normalized error bars illustrating the confidence measure, are plotted in Fig. 4. In these graphs, each bar represents the 10% threshold value of an indicator from a specific data set normalized by the mean value of that indicator over all of the data sets. The bars have been grouped by nonlinear indicator to facilitate comparison. The mean value of each indicator used in the normalization has also been provided above the corresponding group of bars.

Notice that, for some of the bars, the confidence measures are very small, barely being seen about the principal value. These small error bars appear to correspond to the nonlinear indicator flattening out with the applied drive-voltage. Such indicators would be more sensitive to measurement error when estimating the amount of nonlinear distortion and, hence, may not be a good choice for an indicator. Furthermore, the p_{avg} results for the third data set in each group have not been plotted because the linear extrapolation error in p_{avg} never exceeded 10% for this data set; hence, a threshold could not be found.

DISCUSSION AND CONCLUSIONS

Now that the threshold values for the different indices have been determined, we can evaluate the proposed indices on their ability to consistently and reliably distinguish between linear and nonlinear distorted pulses. To be consistent, the indicator should have the same threshold value, within the confidence error bars shown in Fig. 4, for all seven of the data sets. As well as being consistent between data sets, the successful indicator would also be well-behaved within each data set. This means that the nonlinear indicator could only achieve the threshold value at the threshold error setting. Hence, for the indicators considered herein, the ideal indicator would be strictly monotonically increasing.

It is clear that none of the indicators are consistent (Fig. 4). This is particularly evident for extrapolation of the p_{avg} values that have the largest variation in their threshold values. A possible explanation for the lack of consistency can be found by comparing the behavior of the focal pressures for a couple of the data sets. The plots in Fig. 5 are the measured pressure values from the focus for the (a) $\sim$ 5.5-MHz *f*# of 1 transducer, the (b) $\sim$ 5.5-MHz *f*# of 2 transducer, and the (c) $\sim$ 8-MHz *f*# of 1 transducer evaluated in this study. The diameter of all

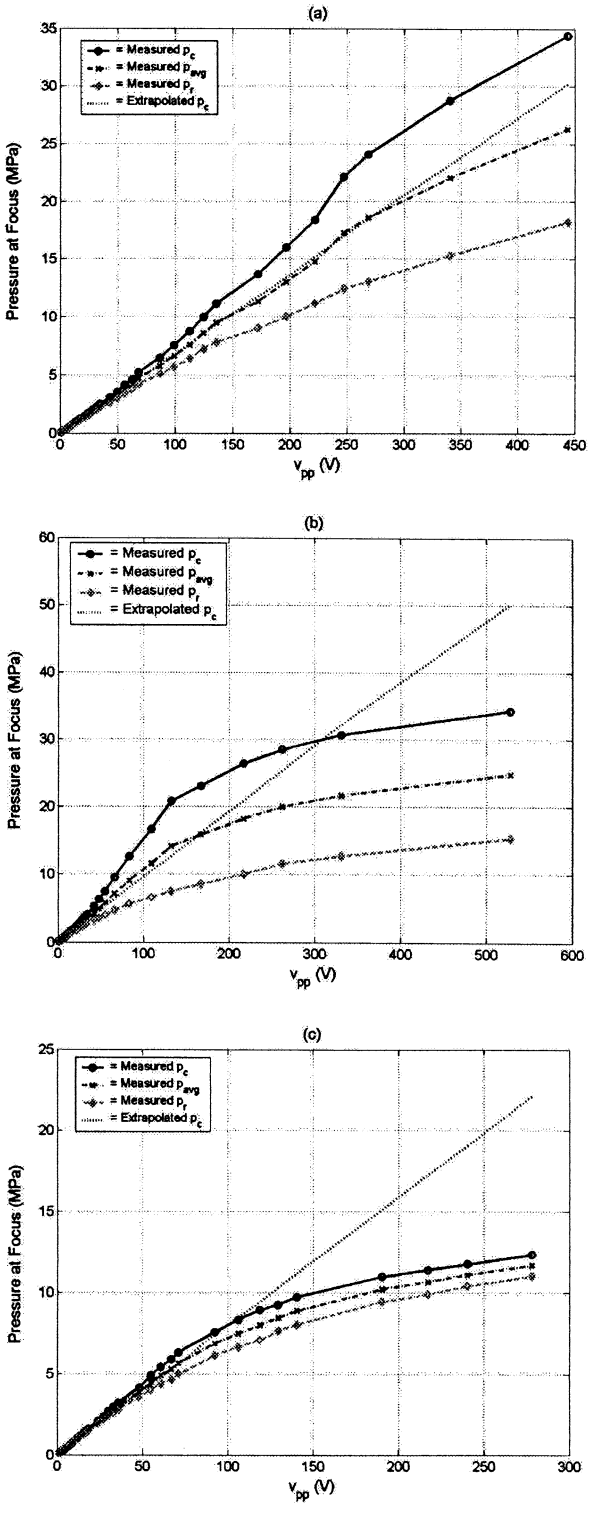

Fig. 5. Direct comparison of pressures at the focus. (a) $\sim$ 5.5-MHz *f*# of 1 transducer, (b) $\sim$ 5.5-MHz *f*# of 2 transducer, and (c) $\sim$ 8-MHz *f*# of 1 transducer. The line in each plot corresponds to a forward extrapolation from the pressures measured at the lowest applied voltage.

three transducers is 1.905 cm, and each is excited by a three-cycle positive-going waveform.

Notice that in all three plots, p_c initially increases away from the linear forward extrapolation line due to asymmetrical distortion. However, as nonlinear absorption increases and the transducer approaches saturation, the p_c values approach the extrapolation line once again and even cross the line in Fig. 5b and c. Although this general trend is observed in all three plots of Fig. 5, the separation between the onset of nonlinearity where the p_c value first moves above the line and the re-crossing of the extrapolation line does not remain the same. The relative importance of nonlinear absorption to asymmetrical distortion seems to increase as the *f*# and frequency increase with a stronger dependence on the frequency.

The above analysis can also be extended to the p_{avg} values. Notice that, in Fig. 5b, the p_{avg} value also increases away from the extrapolation, only to later cross at a higher drive-voltage value. Many of the data sets analyzed exhibited this same type of behavior in the p_{avg} values, so plot (b) is not an unusual exception. However, in Figs. 5a and c, the p_{avg} value never increased above the extrapolation line, but simply drops below the line as the voltage increases. This effect would probably also be present for p_c for some transducers because this is just a natural extension of the trend in the separation between the onset of nonlinearity and the re-crossing of the extrapolation line that was discussed in the previous paragraph. However, in the p_{avg} case, there is no longer a connection between the separation and the *f*# or frequency. Recall that the p_{avg} values depend on both the p_c values and the p_r values. Therefore, the lack of a connection implies that the relative importance of nonlinear absorption and asymmetrical distortion for the p_r values must also be affected by the *f*# and frequency in a similar manner as they were affected for the p_c values.

When the different indicators were defined, not one of the indicators attempted to capture the effects of both nonlinear absorption and asymmetrical distortion. Ostrovskii/Sutin's σ_s focused on asymmetrical distortion with the neglecting of nonlinear absorption, and Bacon's σ_m neglected distortion and focused on nonlinear absorption effects. The frequency-domain indices, such as *si*, could potentially capture both effects, but are not based on a quantitative theory, so there is no guarantee on their performance. Hence, the change in the relative importance of the two nonlinear effects of asymmetrical distortion and nonlinear absorption is what generates the inconsistency in the nonlinear indicators. Therefore, although none of the current indicators are consistent, it may be possible to find a consistent indicator by further developing the theory to include both effects.

Acknowledgments—This work was supported by the NIH (Grant HL58218) and by a DoD Fellowship awarded to T. A. Bigelow. Also, some of the indicators the authors have investigated are under discussion within Working group 14 of IEC Technical Committee 87, as part of a project under the title "*In situ* exposure estimation in finite amplitude beams." The authors also thank Drs. Francis A. Duck and Thomas L. Szabo for useful suggestions.

REFERENCES

AUIM/NEMA. Acoustic output measurement standard for diagnostic ultrasound equipment: Am Institute of Ultrasound in Medicine and Rosslyn, VA. Laurel, MD: National Electrical Manufacturers Association, 1998.

Bacon DR. Finite amplitude distortion of the pulsed fields used in diagnostic ultrasound. Ultrasound Med Biol 1984;10(2):189–195.

Bechmann R, Fair IE. Standard definitions, and methods of measurement for piezoelectric vibrators;177. New York: Institute of Electrical and Electronics Engineers, Inc., 1966.

Bigelow TA, Experimental evaluation of nonlinear indices for ultrasound transducer characterizations. M.S. thesis. University of Illinois at Urbana-Champaign, 2001.

Christopher T, Carstensen EL. Finite amplitude distortion and its relationship to linear derating formulae for diagnostic ultrasound systems. Ultrasound Med Biol 1996;22(8):1103–1116.

Duck FA. Estimating in situ exposure in the presence of acoustic nonlinearity. J Ultrasound Med 1999;18:43–53.

FDA. Information for manufacturers seeking marketing clearance of diagnostic ultrasound systems, and transducer. Rockville, MD: Center for Devices, and Radiological Health, US Food, and Drug Administration, 1997.

Hamilton MF, Blackstock DT. Nonlinear acoustics. San Diego, CA: Academic Press, 1998.

Lucas BG, Muir TG. Field of a finite-amplitude focusing source. J Acoust Soc Am 1983;74(5):1522–1528.

Naugolnykh K, Ostrovsky L. Nonlinear wave processes in acoustics. New York: Cambridge University Press, 1998.

Ostrovskii LA, Sutin AM. Focusing of finite-amplitude acoustic waves. Sov Phys Dokl 1975;20(4):275–277.

Pierce AD. Acoustics. An introduction to its physical principles and applications. Woodbury, NY: Acoustical Society of America, 1991.

Sempsrott JM, O'Brien WD. Experimental verification of acoustic saturation. Proceedings of the1999 IEEE Ultrasonics Symposium, 1999:287–1290.

Sempsrott JM Experimental evaluation of acoustic saturation. M.S. thesis. University of Illinois at Urbana-Champaign, 2000.

Sutin AM. Influence of nonlinear effects on the properties of acoustic focusing systems. Sov Phys Acoust 1978;24(4):334–339.

Szabo TL, Clougherty FC, Grossman CG. Effects of nonlinearity on the estimation of in situ values of acoustic output parameters. J Ultrasound Med 1999;18:33–41.